Computational Design for Digitally Fabricated 3D Inductive Power Transfer Coils

Xu, J.; Doubrovski, E.L.; Geraedts, Jo M.P.; Song, Y.

DOI
10.1115/1.4053500

Publication date
2022

Document Version
Final published version

Published in
Journal of Computing and Information Science in Engineering

Jun Xu
Faculty of Industrial Design Engineering,
Delft University of Technology,
Landbergstraat 15,
2628 CE Delft, The Netherlands
e-mail: J.Xu-6@tudelft.nl

E. (Zjenja) L. Doubrovski
Faculty of Industrial Design Engineering,
Delft University of Technology,
Landbergstraat 15,
2628 CE Delft, The Netherlands
e-mail: E.L.Doubrovski@tudelft.nl

Jo M. P. Geraedts
Faculty of Industrial Design Engineering,
Delft University of Technology,
Landbergstraat 15,
2628 CE Delft, The Netherlands
e-mail: j.m.p.geraedts@tudelft.nl

Yu (Wolf) Song
Faculty of Industrial Design Engineering,
Delft University of Technology,
Landbergstraat 15,
2628 CE Delft, The Netherlands
e-mail: y.song@tudelft.nl

Computational Design for Digitally Fabricated 3D Inductive Power Transfer Coils

The geometric shapes and the relative position of coils influence the performance of a three-dimensional (3D) inductive power transfer system. In this paper, we propose a coil design method for specifying the positions and the 3D shapes of a pair of coils to transmit the desired power. Given region of interests (ROIs) for designing the transmitter and the receiver coils on two surfaces, the transmitter coil is generated around the center of its ROI. The center of the receiver coil is estimated as a random seed position in the corresponding 3D surface. At this position, we use the heatmap method with electromagnetic constraints to iteratively extend the coil until the desired power can be transferred via the set of coils. In each step, the shape of the extension, i.e., a new turn of the receiver coil, is found as a spiral curve based on the convex hulls of the 2D projected adjacent turns along their normal direction. Then, the optimal position of the receiver coil is found by maximizing the efficiency of the system. In the next step, the position and the shape of the transmitter coil are optimized based on the fixed receiver coil using the same method. This optimization process iterates until an optimum is reached. Simulations and experiments with digitally fabricated prototypes were conducted and the effectiveness of the proposed 3D coil design method was verified. [DOI: 10.1115/1.4053500]

Keywords: computer aided design, physics-based simulations

1 Introduction

Wireless power transfer (WPT) has attracted a wide range of interests in the past decade [1]. Among different techniques, inductive power transfer (IPT) is a popular mechanism in near-field WPT, and it was adopted for many applications, e.g., the quite interesting (QI) standard [2]. In an IPT system, a pair of 2D planar spiral coils, one or two layers each, are often used. The power that the system can transmit and the efficiency of the transmission highly depend on the geometric shapes, the materials, the relative positions of the transmitter and the receiver coils. For instance, large misalignment in the lateral and/or increased distance between coils in the axial directions may lead to a significant reduction of the coupling factor of an IPT system [3].

The geometric design methods of 2D planar coils have been well developed in the past decades. However, the forms of products do not always contain a planar surface for embedding a 2D coil. For instance, in personalized product designs, the shape of the product should adapt to certain part(s) of the body, such as wearable electronics [4], stretchable electrodes [5], smart skin [6,7], and microhairy sensor [8]. Embedding a planar coil in such a design may require additional space and/or create large lateral misalignments between the transmitter and the receiver coils. Especially when the receiver coil is small, a significant loss of magnetic flux during the power transfer may happen due to minor misalignments, which may result in an underpowered system [9]. Recent development in soft robotics [10] and electronic skins [11] post even more challenges on integrating IPT in the design as the geometric shapes of these products contain many freeform surfaces, and they may change overtime to achieve different functions.

Technology advancement offers new ways in designing and manufacturing coils for IPT in 3D, such as 3D printing [12,13], stamp printing [14], cartan transfer printing [15], etc. For instance, Jeong et al. [16] integrated a IPT system in a smartwatch strap with flexible 2D coils and magnetic field shielding materials. Researchers also developed new inductors [17], sensors [18,19], etc. using 3D printed electronics. However, regarding coils for IPT, most of the designs were achieved by simply projecting, or morphing, a 2D spiral/rectangular pattern to a 3D surface(s). The spatial relations between the transmitter and receiver coils, the distances between each turn of a coil, and the influence of 3D shapes on the electromagnetic field of the IPT system were not fully considered in the design of these coils.

In this paper, we address this gap by introducing a new approach for designing the geometric shapes of 3D coils for IPT. The scientific contribution is that in given region of interests (ROIs), we embed both geometric and electromagnetic constraints in the design of the smallest possible pair of 3D coils to achieve transmitting the desired power. The proposed approach was verified by FEM simulations and experiments on digitally fabricated coils.

This paper is based on earlier work [20] published in ASME IDETC/CIE 2021 conference. The remainder of the paper is arranged as follows: in Sec. 2, a brief literature review was given on different aspects regarding coil design and manufacturing for IPT. Section 3 introduces the proposed approach and in Sec. 4, we present three cases to compare the calculation, the simulation, and the experiment results for verifying the approach. Finally, a short conclusion is presented.

2 Literature Review

2.1 Requirements of Coils. IPT can be used in a variety of products and therefore coils will have to be designed with different shapes and using different materials, e.g., a pair of cylindrical coils with magnet wires is often used for charging the toothbrush [21]. Among different shapes, a pair of 2D planar circular, or rectangular, spiral coils is the most common pattern(s) used in an IPT system. The advantage of using planar circular coils is that a pair of them has higher self- and mutual-inductances than square shaped coils with the precondition that the length of conductors is the same

Contributed by the Computers and Information Division of ASME for publication in the Journal of Computing and Information Science in Engineering. Manuscript received August 22, 2021; final manuscript received January 6, 2022; published online March 4, 2022. Assoc. Editor: Paul Witherell.

[22]. However, in many designs, the design space of the coil is often a rectangular shape. Using a rectangular spiral coil may achieve a larger inductance than using the circular spiral coil given a defined rectangular design space [23]. Coils in other shapes, e.g., elliptical coils, are also reported in the literature for specific applications [24,25]. No matter which shape is used in an IPT system; coils are often winded in the convex and close-packed forms for reducing the volume and enlarging the self- (and/or mutual) inductance of the coil(s).

With a pair of coils, the maximal efficiency of an IPT system can be described as

$$\eta_{\max} = K_{12}^2 Q_1 Q_2 \Big/ \left(1 + \sqrt{1 + K_{12}^2 Q_1 Q_2}\right)^2 \tag{1}$$

and the maximum achievable power to be transferred by this system is [26]

$$P_{\text{out}-\max} = \frac{K_{12} Q_1 Q_2 R_1 R_2 R_L V^2}{(R_1(R_2 + R_L) + K_{12} Q_1 Q_2 R_1 R_2)^2} \tag{2}$$

Here, the quality factors $Q_1 = 2\pi f L_1/R_1$ and $Q_2 = 2\pi f L_2/R_2$ are the figure-of-merit of the transmitter and the receiver coils, respectively [27]. L_1 and L_2 are the self-inductance of these two coils, and R_1, R_2, and R_L are the resistances of the transmitter coil, the receiver coil, and the load, respectively [3]. The coupling factor between two coils $K_{12} = M_{12}/\sqrt{L_1 L_2}$, where M_{12} is the mutual-inductance between the transmitter and the receiver coils.

Given the design of a pair of coils for an IPT system, according to these definitions, the geometric shapes of the coils might influence the self-inductances and the resistance of these two coils. The relative position might influence the mutual-inductances between them and the efficiency of the system, e.g., the angular, lateral, and axial misalignments of these two coils often lead to a significant loss of power to be transmitted. In general, for transmitting a given amount of power using IPT, a pair of well aligned coils with large self-inductances and lower resistances is preferred for minimizing the geometric sizes of the coils in the design space, and therefore saving material and manufacturing cost of the coils as well.

2.2 Printing Electronics. Coils are often wound using litz wires [28]. With the development of printed electronics, printable conductive inks have been used to replace conventional conductors in many IPT applications for saving the cost and/or reducing the size while providing enough power for the system [29]. 2D printed electronics, i.e., printing a single layer or multiple layers of silver ink on the substrate, was first introduced for designing low power IPT systems [16]. Conformal printing is often used for translating those 2D designs to 3D application based on the flexibility of the conductive ink and the substrate. In conformal printing, electronic structures are first fabricated on a flat flexible substrate by inkjet printing or screen printing; the print is then deformed to the target (curved) surface using different manufacturing methods [30]. For instance, Harnois et al. [31] fabricated frequency selective surface structures on a 2D planar polyethylene terephthalate substrate. The 2D surface was then bonded onto a 3D surface. Devaraj and Malhotra [32] proposed a new process that can transform flat printed circuits on thermoplastic sheets into freeform interconnect–polymer assemblies and integrated them with a desired 3D surface. A number of studies have confirmed that thermoforming technology can also be used for deforming the printed large-area interconnect circuits towards the desired shape [33]. Similarly, by combining the in-mold decoration technique and 3D printed electronics, in-mold electronics was also widely adopted by industries for manufacturing functional electronics [34].

Direct ink writing is another way of digitally fabricating electrical circuits in 3D [15]. For instance, Zhou et al. [35] fabricated a broad array of 3D radio frequency passive components (e.g., inductors, capacitors, etc.) for chip-scale radio frequency electronics. Using 3D printed electronics, Boekraad [36] succeeded in printing a coil onto a curved surface using a set of non-planar toolpaths. However, it might be difficult to generalize this approach to other applications, especially for printing on freeform surfaces. Zhu et al. [37] developed an on-site 3D electronics printing technique to print sensors as well as a coil for WPT on human hands. Recently, Hou et al. [3,38] mapped 2D rectangular/circular spiral patterns to arbitrary freeform surfaces for generating 3D coils and validated the effectiveness and efficiency of using those coils in the IPT system based on 3D printed electronics.

2.3 Design for Digitally Fabricated 3D Coils. When using printed electronics for IPT, coils are often designed in 2D using the circular/rectangular spiral patterns with the step size (distance between turns) as the sum of the width of the printing trace and a specified clearance between each turn of the coil. However, in the use of the IPT system, those 2D designs are either deformed by the users following particular usage scenarios, e.g., flexible electronics [16], or mapped to a 3D shape using a specific type of mapping [38]. Either might change the geometry and/or the relative position of (each turn of) the coils, leading to a decrease in performance of the IPT system. For instance, the distances between different turns of a coil might change by projecting a 2D design on a 3D curved surface [39]. This might waste the design space or result in a potential risk of short circuits between turns. Another potential issue is that a convex 2D coil might become concave after mapping it to 3D, which will decrease the performance of the IPT system.

Designing coils in 3D can avoid those problems. In the area of computer aided design (CAD), researchers developed many algorithms that can be used in 3D coil design. For instance, the fast marching [40] and the heatmap [41] are two typical algorithms to generate concentric patterns regarding the geodesic distance on the freeform surface. Another example is a new type of five-axis spiral inspection path generation strategy which is able to create a uniform toolpath regarding the geodesic distance [42]. The designed 3D coils can be manufactured using the direct ink writing technique in 3D or using the conformal printing technique by mapping the 3D design to 2D, e.g., by the least-square conformal map (LSCM) [43–45]. However, extensive literature study did not reveal existing research works that integrate the electromagnetic requirements of coils for designing and manufacturing IPT system on a freeform 3D surface.

3 The Approach

Given a desired amount of power to be transferred via the IPT system, we propose a 3D coils design approach as Fig. 1. In the first step, two ROIs are specified on two surfaces where the IPT system is supposed to be integrated. A transmitter coil is then generated at an initial position either specified by the designer or at the center of a surface. At first, the size of this coil will only be limited by the boundary of the ROI, i.e., an excessively large transmitter coil will be generated in step 2. Then, a random seed for the receiver coil on the corresponding surface is specified. Using this seed, we grow the receiver coil turn by turn until the size that the system is able to transmit the desired power. The position of the seed of the receiver coil is further optimized until the maximal efficiency is achieved as step 3. In step 4, we flip the order and used the receiver coil to optimize the position and the shape of the transmitter coil based on the desired power to be transferred. Steps 3 and 4 iterate until the changes of the geometric centers of both coils (step 5) are less than a threshold. In the following, details of the above steps are explained.

3.1 Region of Interest and the Transmitter Coil. In the design of 3D coils, a design space, i.e., the ROIs for the transmitter

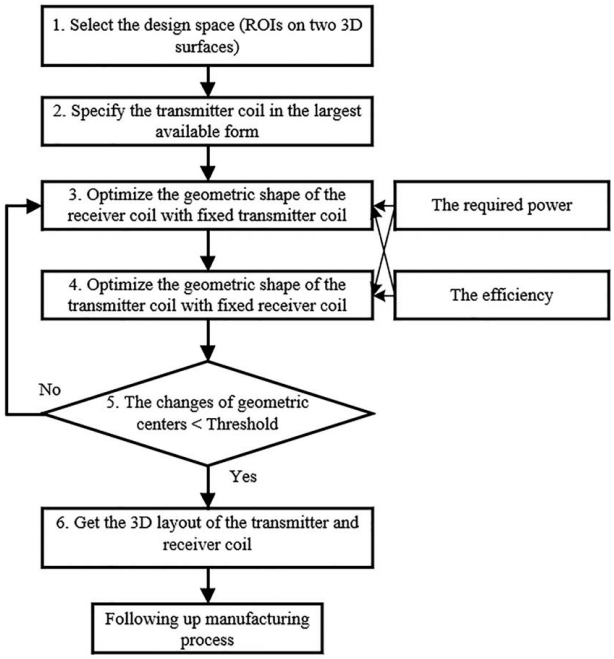

Fig. 1 The approach for designing 3D coils for IPT

and the receiver coils, are specified first as

$$S_T(u, v)|u, v \in (0, 1) \tag{3}$$

and

$$S_R(u, v)|u, v \in (0, 1) \tag{4}$$

respectively. In $S_T(u, v)$, an initial position of the transmitter coil is specified as $S_T(0.5, 0.5)$ as the center point in Fig. 2. Here we take the UV center of the surface as the seed position but in practices, any points on $S_T(u, v)$ can be used. A geodesic offset of the seed point $C_0(u)|u \in (0, 1)$, which is computed based on the heatmap method [46], is used as the starting ring of the coil as shown in Fig. 2. Here the offset value is defined as 120% of the width of the coil trace (20% clearance, 0.6 mm in this paper).

Using $C_0(u)$ as the basis of the inner turn of the transmitter coil, the basis of the next turn $C_1(u)$ of the coil is computed using the geodesic offset with the same offset value. Here, the shapes of the $C_0(u)$ and $C_1(u)$ may influence the performance of the I system. For instance, the direction of the electromagnetic fields of a coil follows the right-hand rule regarding the direction of the current that flows through it, and in the concave area, the current might generate "negative" electromagnetic fields which will result

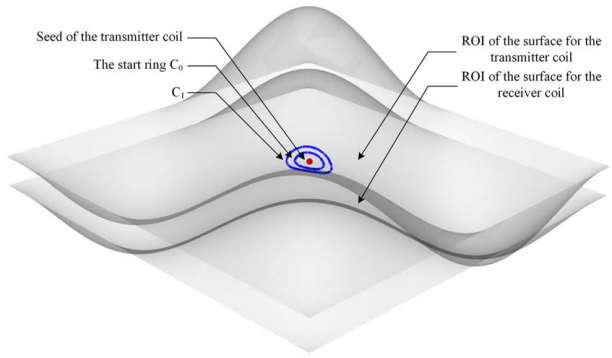

Fig. 2 ROI and the initial positions of the transmitter coil

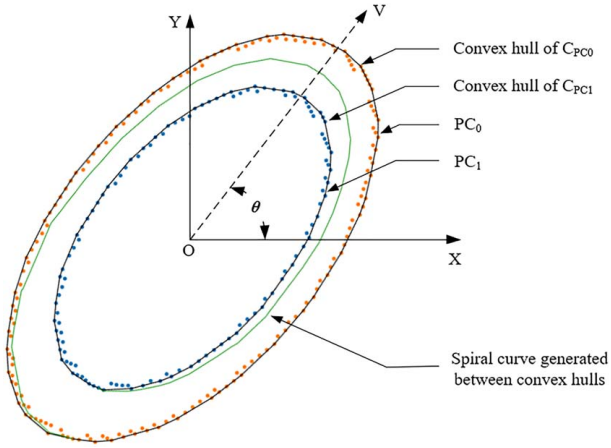

Fig. 3 Project curves in 2D, convex hull, and the generated spiral curve

in a decreased "total" electromagnetic field. Therefore, concave regions of $C_0(u)$ and $C_1(u)$ should be avoided.

A way to avoid potential concave regions in $C_0(u)$ and $C_1(u)$ is to use the convex hull(s) of the projected shapes in their best-fit plane. For this, two curves are discretized first as pointsets $P_0 = \{P_0(i)|i = 0 \ldots m_1\}$ and $P_1 = \{P_1(i)|i = 0 \ldots m_2\}$, respectively. Then a superset $P_{01} = \{P_{01}(i)|i = 0 \ldots m_3\}$ can be acquired as $P_{01} = P_0 \cup P_1$. A best-fit plane $(c, \boldsymbol{n})$ of this superset P_{01} can be generated as

$$\arg\min_{\|\boldsymbol{n}\|=1} \sum_{i=0}^{m_3} ((P_{01}(i) - c)^T \boldsymbol{n})^2 \tag{5}$$

where c is the geometric center of $P_{01}(i)$ and $c = \sum_{i=0}^{m_3} P_{01}(i)/m_3$. $\mathbf{n}$ is the normal direction of the plane. With the found $\boldsymbol{n}$, P_0 and P_1 are projected to plane $(c, \boldsymbol{n})$ as

$$PC_0 = \{(P_0(i) - c) - ((P_0(i) - c) \cdot \boldsymbol{n}^T) \cdot \boldsymbol{n} |\ i = 0 \ldots m_1\} \tag{6}$$

and

$$PC_1 = \{(P_1(i) - c) - ((P_1(i) - c) \cdot \boldsymbol{n}^T) \cdot \boldsymbol{n} |\ i = 0 \ldots m_2\} \tag{7}$$

Figure 3 depicts the PC_0 and PC_1 on the projected plane. To remove possible concave regions in these two contours, the convex hulls C_{pc0} and C_{pc1} [47] of them are calculated as shown in Fig. 3. A 2D spiral curve is then generated by rotating a vector V around the geometric center of C_{pc0} and C_{pc1} as

$$\text{Sprial}(\theta) = \left\{ \left. \begin{array}{l} \left(1 - \dfrac{\theta}{2\pi}\right) C_{pc0} \cap V(\theta) + \\ \dfrac{\theta}{2\pi} C_{pc1} \cap V(\theta) \end{array} \right| \theta = 0 \ldots 2\pi \right\} \tag{8}$$

where $V(\theta)$ stands for a vector from the origin point towards $(\cos(\theta), \sin(\theta))$ and $\cap$ is used to find the intersection between two lines/curves.

After $Sprial(\theta)$ is acquired, we project the Sprial(θ) and C_{pc1} back to the $S_T(u, v)$, where the projected Sprial(θ) is the extension, i.e., a new turn, of the transmitted coil and the projected C_{pc1} is the basis for the next new turn. This process iterates until the boundary of ROI is reached. Finally, the transmitter coil $c_t(u)$ is constructed based on a piecewise curve where each piece is the projected Sprial(θ) regarding this turn. In this case, the transmitter coil is generated with an excessively large size as the starting point of the optimization process as shown in Fig. 4.

3.2 Optimize Geometry of the Receiver Coil. Given a starting position $S_R(a, b)$, a receiver coil $c_r(u)$ can be generated

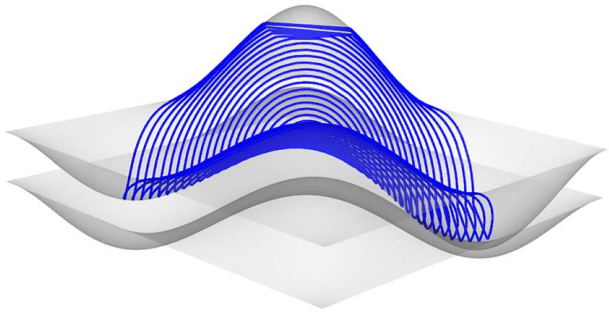

Fig. 4 The generated transmitter coil where the last turn reaches the boundary of the ROI

in $S_R(u, v)$ using the same strategy as described in the previous section with an exception, which is the power to be transmitted. For designing a 3D coil with the minimal size, the desired power to be transferred (or with an additional threshold) will be used as the upper limit, i.e., the extension of the coil will stop when such a limit is reached. Equation (2) defines the maximal amount of power that the system can transfer. In the equation, it can be found that this limit is influenced by the mutual- and self-inductances of the coils, the resistance of the coil, and the resistance of the load.

Suppose the shape of the cross section of the printed trace is rectangular, the resistances of the transmitter $c_t(u)|u \in (0, 1)$ and the receiver coils $c_r(u)|u \in (0, 1)$ in Eq. (2) can be represented as

$$R_{t/r} = \rho \int_{u=0}^{1} c_{t/r}(u)du/(WH) \tag{9}$$

where W is the width and H is the height of the printed trace, respectively. ρ is the volume resistivity of the printed conductive ink (after curing). $c_{t/r}$ means this equation can be used for either $c_t(u)$ or $c_r(u)$. Silver inks are often used in printed electronics. Most silver inks have a relatively larger resistivity than that of the pure silver or copper. For instance, the volume resistivity of the pure copper is about $1.68 \times 10^{-8}\ \Omega$ m where for a typical silver ink, it is about $3 \times 10^{-7}\ \Omega$ m. Therefore, the power that the printed coils can be transmitted is often limited compared to the same size coils made of litz wires.

Previous research [3,48] indicates that the mutual-inductance between the 3D transmitter and receiver coils can be calculated using Neumann's formula as

$$M = \frac{\mu_0}{4\pi} \oint_{C_t} \oint_{C_r} \frac{\overrightarrow{dc_t} * \overrightarrow{dc_r}}{D} \tag{10}$$

where μ_0 is the magnetic permeability of the vacuum ($4\pi \times 10^{-7}$ H/m). c_t and c_r are the contours of the transmitter and the receiver coils, respectively. D is the distance between dc_t and dc_r. The self-inductance of the 3D coils can be calculated as the sum of the external inductance and the internal inductance as

$$L_{t/r} = \frac{(M_{\text{mid-inn}} + M_{\text{mid-out}})}{2} + \frac{\mu_0}{8\pi} \int_0^1 c_{t/r}(u)' du \tag{11}$$

where $M_{mid-inn}$ is the mutual-inductance between the centerline and t inner edge of $c_{t/r}$, and $M_{mid-out}$ is the mutual-inductance between the centerline and the outer edge of $c_{t/r}$. Details of the calculation process can be found in Ref. [38].

With a fixed input voltage and a fixed load resistance, combine Eqs. (9)–(11) with Eqs. (1) and (2), the maximal power that can be transferred by the IPT can be simplified as

$$P_{\text{out-max}} = \frac{4\pi^2 f^2 M(a,b) L_T(a,b)^{3/2} L_R(a,b)^{3/2} R_L V^2}{16\pi^4 f^4 M(a,b)^2 L_T(a,b)^3 L_R(a,b)^3 + 2(R_t(a,b)R_r(a,b) + R_t(a,b)R_L + 1)4\pi^2 f^2 M(a,b) L_T(a,b)^{3/2} L_R(a,b)^{3/2} + (R_t(a,b)R_r(a,b) + R_t(a,b)R_L)^2} \tag{12}$$

where $M(a, b) = M(c_t(PC_0(S_T(a, b)), PC_1(S_T(a, b))), c_r(PC_0(S_R(a, b)), PC_1(S_R(a, b)))), L_T(a, b) = L(c_T(PC_0(S_T(a, b)), PC_1(S_T(a, b)))),$ and $L_R(a, b) = L(c_r(PC_0(S_R(a, b)), PC_1(S_R(a, b))))$. Equation (12) can be simplified as $P_{\text{out-max}} = f_{\text{power}}(a, b)$, and it is used as the termination condition in the receiver coil generation. Similarly, the efficiency of the system can be denoted as

$$\eta_{\max} = \frac{4\pi^2 f^2 M(a,b)^2}{R_t(a,b)R_r(a,b) + (R_t(a,b)^2 R_r(a,b)^2 + 4\pi^2 f^2 M(a,b)^2 R_t(a,b)R_r(a,b))^{1/2}} \tag{13}$$

Equation (13) can also be simplified as $\eta_{\max} = f_{\text{efficiency}}(a, b)$. The center position of the receiver coil $S_R(a, b)$ can be found by maximizing the efficiency of the system as

$$\arg \max_{a,b \in (0,1)} f_{\text{efficiency}}(a, b) \tag{14}$$

Based on Eqs. (12) and (14), a receiver which is able to transfer the desired power with maximal efficiency can be generated. Figure 5(*a*) presents the generated optimal receiver coil regarding the transmitter coil. It can be found that though the transmitter coil is large, the size of the receiver coil is much smaller, as it is limited by the amount of power to be transferred.

3.3 Iterative Optimization. With the generated receiver coil, following the proposed approach, we fix the receiver coil and use the same strategy as Sec. 3.3 to find an optimal transmitter coil. This optimization process iterates until in the kth iteration, both the distance between the center of the receiver coil $S_R^k(a, b)$ and the optimized $S_R^{k+1}(a, b)$ using Eq. (14) and the distance between the transmitter coil $S_T^k(a, b)$ and the optimized $S_T^{k+1}(a, b)$ using Eq. (14) are less than a threshold, e.g., 0.1 mm. In Figs. 5(*b*) and 5(*c*), several steps in such iterative optimization process are presented.

4 Experiments

In this section, we present the results of three experiments to verify the proposed approach. In the first experiment, the results of the calculation, the simulation, and the measurements on a prototype are compared. Then we explore the possibility of designing the IPT system for a shaver by comparing the calculation and simulation results. In the third experiment, using the proposed methods, we printed a coil on the liner of a hand splint for providing power to measure physiological parameters.

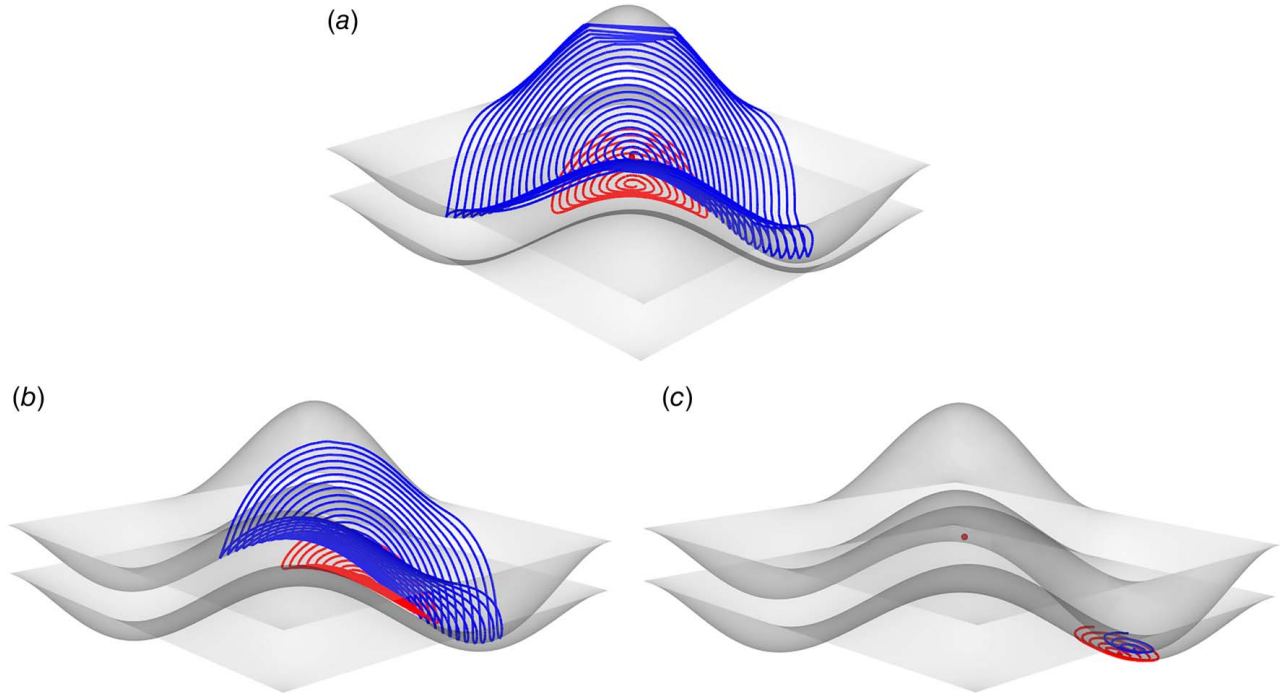

Fig. 5 Process of iterative optimization: (*a*) the transmitter coil (top) and the receiver coil (bottom), (*b*) one of the middle steps of optimization, and (*c*) the final step of optimization

4.1 Design a Pair of Coils on Two Freeform Surfaces. The proposed design approach was implemented by PYTHON using SciPy, NumPy, and the non uniform rational B-spline surface (NURBS) python libraries. Figure 6(*a*) presents six steps in the optimization process of the paraboloid surface case, where each step is further divided into (a) and (b) these two sub-steps, corresponding to using the transmitter coil to optimize the receiver coil and using the optimized receiver coil to optimize the transmitter coil, respectively. In this case, we set the desired power to be transferred as 0.05 Watt to highlight the effects of each turn of the coils. With an Intel™ Core i5™ 3.7GHZ CPU, it took about 35 min to finish each step of the computing. In the figure, it can be found that with the development of the optimization process, the distance between the two coils was reducing, the sizes of both coils were shrinking as well, as only a few turns were enough to transfer the desired power at a shorter distance. In Fig. 6(*b*), the parameters of coils regarding each step are presented, where the length and the resistance of the coils decreased during the optimization process while the power that can be transmitted always met the requirement. In the final several steps, the power that can be transferred increased due to that the turn of the coil was set to be an integer. While the distance between two coils was small and the number of turns was low, an extra turn may lead to large changes of the power that can be transferred. It is worth mentioning that in the proposed approach, the effectiveness of the optimization results highly depends on the ROIs selected by the users and in general, the closer the ROIs of the transmitter and the receiver coils are, the higher the efficiency is. The initial position of the transmitter coil is specified at $S_T(0.5, 0.5)$, and a better initial position based on the prior knowledge of the designer can also accelerate the optimization process.

To further verify the calculation results, we used the ANSYS™ Maxwell™ simulation tool to explore the properties of Eq. (14) at its optimal position. In the simulation, we fixed the transmitter coil but changed a of the center positions $S_R(a, b)$ (along u-axis of the NURBS) from 0.35 to 0.65 with a 0.005 step and b (along v-axis) from 0.50 to 0.80 with a 0.005 step, resulting in 3721 setups. With the same computer, it took about 10 s to finish the simulation of a setup. Figure 7(*a*) presents the relations between those positions and the power that can be transmitted by the coils. It can be found that the maximum was around $S_R(0.485, 0.735)$, which is the optimal position found by the algorithm. It is worth mentioning that the optimal position was not at the center of the figure due to the fact that the boundary of the coils reached the boundary of the ROIs. Figure 7(*b*) presents the magnetic B-field of the IPT system at the optimal position.

To explore the possibility of using the direct printing method to fabricate the coils, we redesigned and fabricated a pair of coils that can transmit 0.1 W power with a 5 Ω resistive load deployed on the receiver side. Figure 8(*a*) presents the design which was printed by an Ultimaker S5 printer with two grooves at the position of the designed coils. The height and width of them were set the same as the parameters of the optimized transmitter and receiver coils, respectively. Silver ink (density: 3700 kg/m^3, volume resistivity: $<3\times10^{-7}$ Ω m) was filled in the groove to create the coils (Fig. 8(*b*)). In Fig. 8(*c*), the transmitter and the receiver coils were placed in the designed relative position to form an IPT system and in Fig. 8(*d*), an light-emitting diode (LED) was lighted using the power transferred by the system.

Table 1 presents the calculated, simulated, and measured properties of the coils presented in Fig. 8. In the table, T stands for the transmitter coil and R represents the receiver coil. Regarding the resistance, for the transmitter coil, it was measured as 0.9 Ω and for the receiver coil, the resistance was about 0.5 Ω. The calculated self-inductance of the optimized transmitter coil was 3.38×10^{-6} H, and the simulation result was 3.35×10^{-6} H while the calculated self-inductance of the optimized receiver coil was 1.39×10^{-6} H, and the simulation result was 1.41×10^{-6} H. The calculation results and the simulation results of the self-inductance of the transmitter coil were 9.8% and 10.6% smaller than the measurement results, respectively. And the calculation result of the self-inductance of the receiver coil was 12% smaller than the measurement result, while the simulation result was 10.8% smaller than the measurement result. At this position, the mutual-inductance of the calculation and the simulation between the optimized coils were 5.94×10^{-7} H and 6.01×10^{-7} H, respectively. The calculation result of the mutual-inductance was 13.8% smaller than the measurement result, while the simulation result was 12.8% smaller than the measurement result. The quality factors of coils

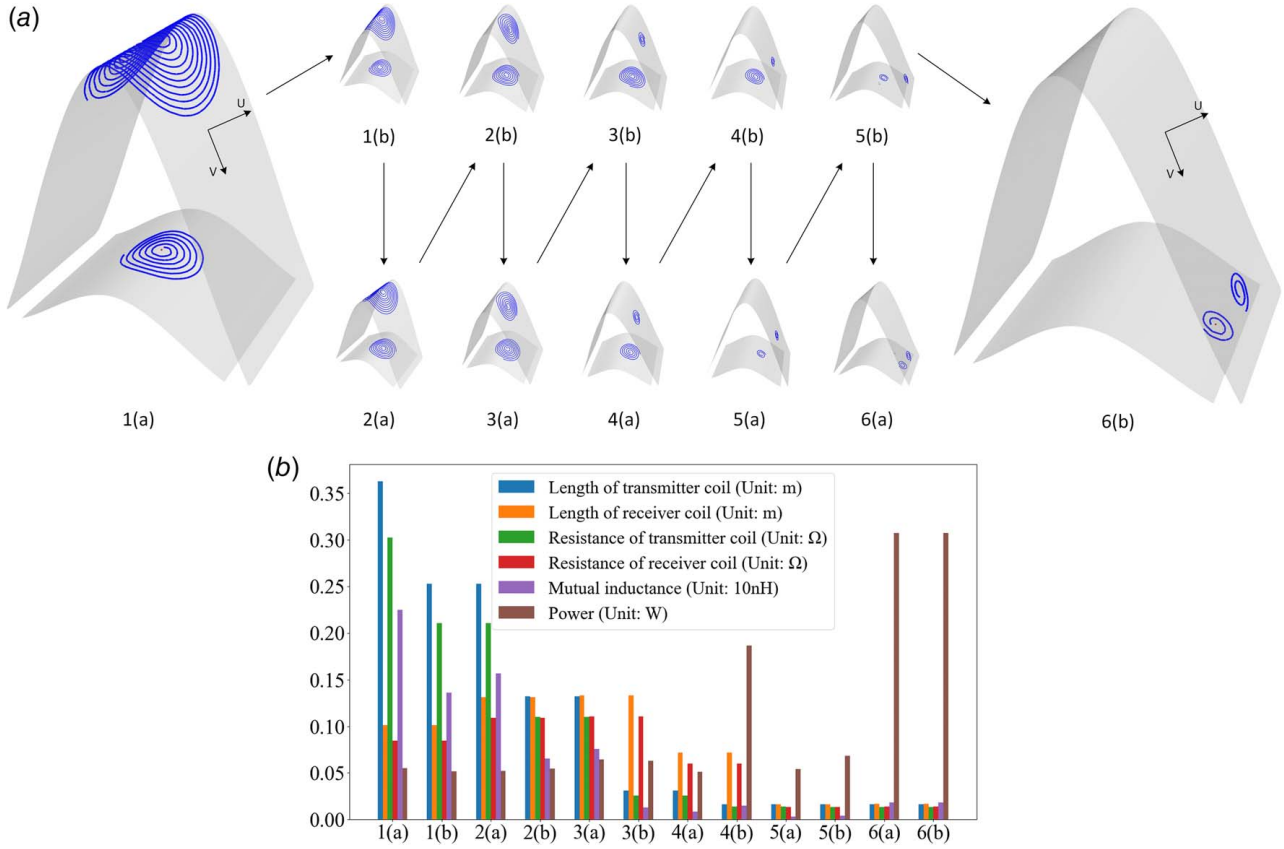

Fig. 6 Design 3D coils: (*a*) the optimization process and (*b*) the lengths and resistances of coils and the power can be transferred for each step in the optimization

were not high, mainly due to the large resistances introduced by the silver ink.

For both the transmitter coil and the receiver coil, errors between the calculation and the simulation results were small, which verified the effectiveness of the proposed approach. However, errors were slightly larger compared to the measurement results. This might be caused by the manual filling process of the silver ink, where the filled silver ink might not be uniformly distributed in the grooves.

To further verify the proposed approach, we designed the transmitter coil regarding a fixed receiver coil using both the proposed approach and the approach introduced by Tao et al. [38], which suggests to map a 2D design to the 3D ROI using UV mapping. To make the two designs comparable, we set the center of both coils at the same position and the power to be transferred as 0.1 W. Figure 9 presents the transmitter coils designed by the two approaches and Table 2 presents calculation results of both designs. Regarding the length of coils, the coil designed by the proposed approach was 0.230 m and the result of Tao's coil was 0.277 m. The shorter length of coil (17%) suggested by the proposed approach reduced the cost of silver ink and might free more space in the ROI for other purposes. If both coils were

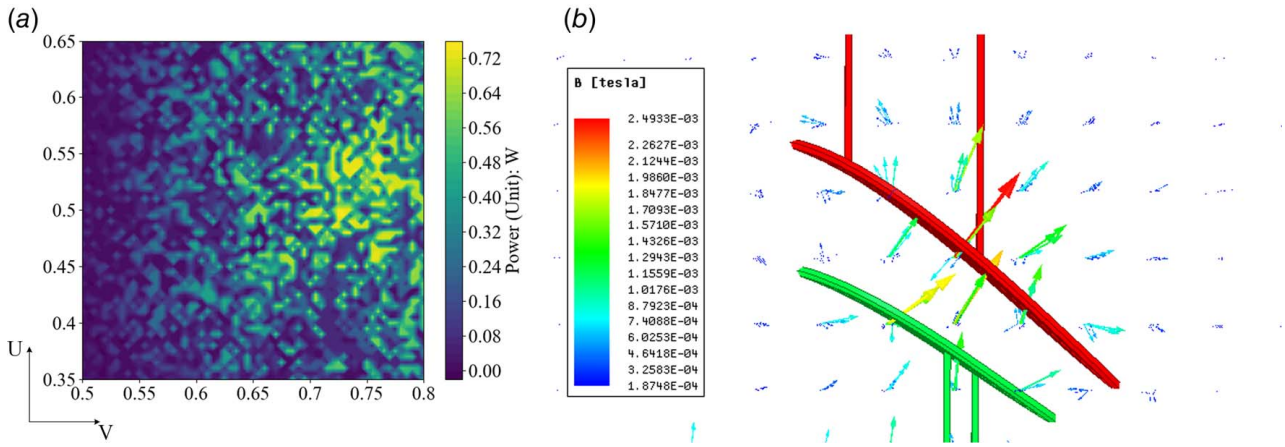

Fig. 7 Simulation results of a pair of optimized coils: (*a*) the relation between position and the power that can be transmitted and (*b*) B-field of the IPT system

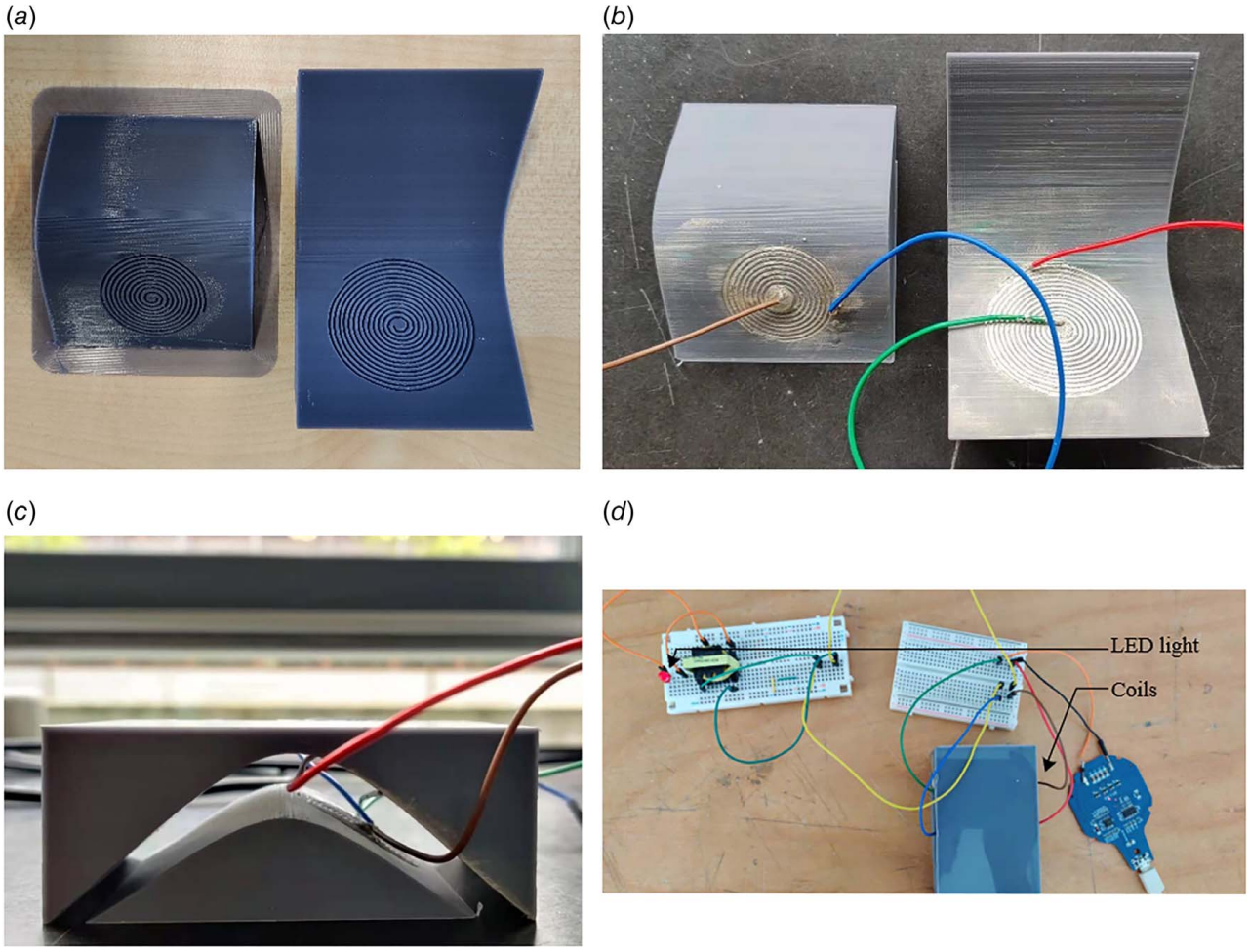

Fig. 8 Fabricated coils by direct printing: (*a*) the model with the groove, (*b*) the fabricated coils, (c) the IPT system, and (*d*) an LED powered by the IPT system

manufactured with the same type of ink and had the same cross-sectional area, the resistances of them were linearly correlated to the lengths. Therefore, the resistance of the coil designed by the proposed approach was also 17% smaller. Though the coil was shorter, the power transmitted by the coil designed by the proposed approach was larger (0.112 W) than that of Tao's approach (0.096 W).

4.2 Design the Inductive Power Transfer System for a Shaver. To evaluate the potential of using the proposed 3D coil design method in design, we redesigned a shaver by integrating an 3D IPT system with the desired power to be transferred as 1 W. Figure 10(*a*) presents the original design of the shaver and holder, where two surfaces were specified as the ROIs for the transmitter coil and the receiver coil, respectively. In the design of the IPT,

Table 1 Measurement results of coils

	T	Error regarding the measurement	*R*	Error regarding the measurement
Resistance (calculated, in Ω)	0.68	−24.4%	0.37	−25.6%
Resistance (simulated, in Ω)	0.72	−20.0%	0.39	−22.2%
Resistance (measured, in Ω)	0.90	–	0.50	–
Self-inductance (calculated, in μH)	3.38	−9.8%	1.39	−12.0%
Self-inductance (simulated, in μH)	3.35	−10.6%	1.41	−10.8%
Self-inductance (measured, in μH)	3.75	–	1.58	–
Quality factor (calculated)	3.13	19.5%	2.35	18.7%
Quality factor (measured)	2.62	–	1.98	–
		Between *T* and *R*		Error regarding the measurement
Mutual-inductance (calculated, in μH)		0.59		−13.8%
Mutual-inductance (simulated, in μH)		0.60		−12.8%
Mutual-inductance (measured, in μH)		0.69		–
Coupling factor (calculated)		0.27		−3.2%
Coupling factor (simulated)		0.28		−1.4%
Coupling factor (measured)		0.28		
Power transfer efficiency			8.5%	

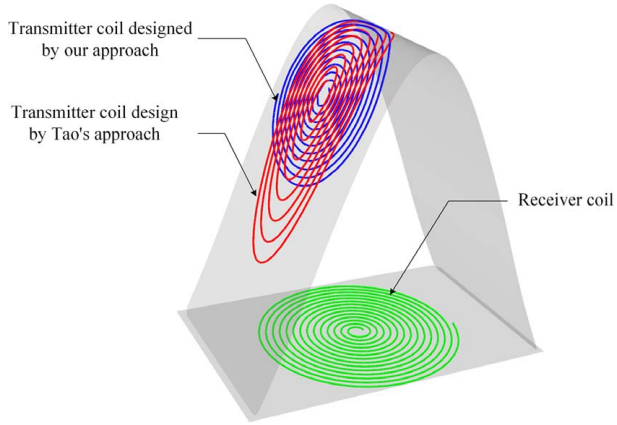

Fig. 9 Transmitter coils designed by Tao's approach and the proposed approach

we set the voltage as 5 V and the load resistance as 5 Ω. Figure 10(*b*) presents the optimized 3D transmitter and the receiver coils. Here, the length of the coil was 0.17 m for both the transmitter coil and the receiver coil. Using this design, the IPT system was able to transmit the power of 1.15 W according to calculation. In Fig. 10(*c*), the simulation results of the 3D IPT are presented where the power can be transmitted was 1.21 W. The absolute error of the power transmitted between the calculation and simulation was 0.06 W (4.96%).

Table 3 presents the calculated and simulated result of the coils presented in Fig. 10. In the table, *T* and *R* represent the transmitter coil and the receiver coil, respectively. The calculated resistance of the optimized receiver coil was 1.40×10^{-1} Ω and the simulation result was 1.43×10^{-1} Ω while the calculated self-inductance of the optimized receiver coil was 1.42×10^{-1} Ω, and the simulation result was 1.46×10^{-1} Ω. Regarding the self-inductance, for the transmitter coil, the calculated result was 3.08×10^{-6} H and the simulated result was 3.15×10^{-6} H, and for the receiver coil, the calculated result was 3.39×10^{-6} H and the simulated result was $3.31 \times$

Table 2 Comparison between Tao's approach and the proposed approach

	Transmitter, by Tao's approach	Transmitter, by the proposed approach	Change regarding Tao's approach
Length (m)	0.28	0.23	−17.00%
Resistance (Ω)	0.19	0.16	−17.00
Self-inductance (μH)	0.54	0.48	−11.10
		Between transmitter and receiver	
Mutual-inductance (nH)	11.37	9.67	−15.00%
Power can be transferred (W)	0.10	0.11	16.34%

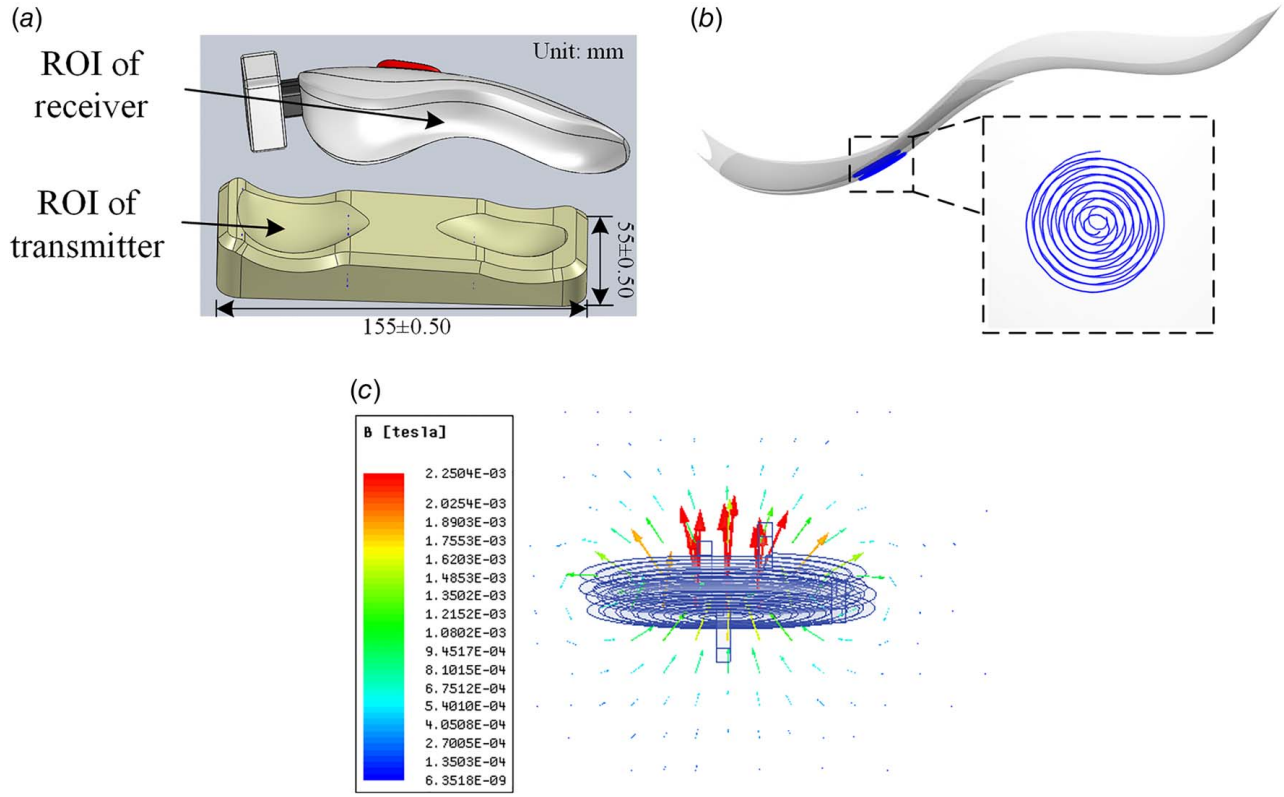

Fig. 10 Design the IPT system of a shaver using the proposed approach: (*a*) the CAD model of the shaver, (*b*) the 3D coil generated on ROI of transmitter, and (*c*) simulation results of the optimized coils

Table 3 Comparison between simulation and calculation

	T	Error regarding the simulation	R	Error regarding the simulation
Resistance (calculated, in Ω)	0.14	−2.00%	0.14	−3.02%
Resistance (simulated, in Ω)	0.14	–	0.15	–
Self-inductance (calculated, in μH)	0.31	−2.46%	0.34	2.48%
Self-inductance (simulated, in μH)	0.32	–	0.33	–
		Between T and R		Error regarding the simulation
Mutual-inductance (calculated, in μH)		0.20		−3.25%
Mutual-inductance (simulated, in μH)		0.21		–
Coupling factor (calculated)		0.62		−3.23%
Coupling factor (simulated)		0.64		–

10^{-6} H. The calculation results were 2.46% smaller than the simulation results. And the calculation result of the self-inductance of the receiver coil was 2.48% bigger than the simulation result. At this position, the mutual-inductance of the calculation and the simulation between the optimized coils were 2.00×10^{-7} H and 2.07×10^{-7} H, respectively. The calculation result of the mutual-inductance was 3.25% smaller than the simulation result.

4.3 Design an Inductive Power Transfer System for Hand Splint. In this section, we present a case of integrating the IPT

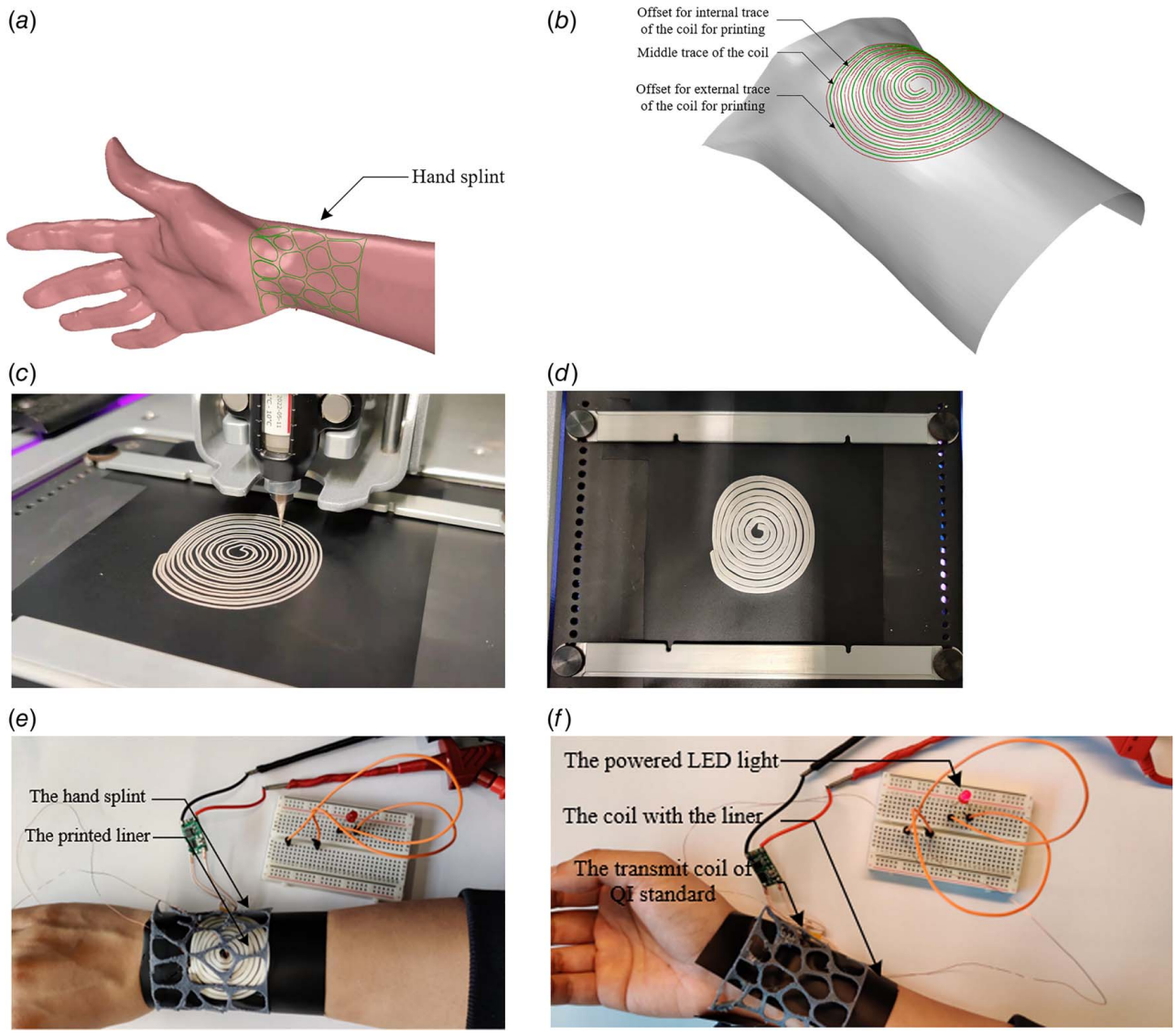

Fig. 11 A smart liner with an integrated IPT system for the hand splint: (*a*) the design of the hand splint, (*b*) the designed coil using the proposed approach, (*c*) the printing process, (*d*) the printed receiver coil, (*e*) the printed liner with the hand splint, and (*f*) power an LED light

system into personalized product design using conformal printing techniques. The case was set to print a smart soft liner of a hand splint for measuring physiological parameters of the hand, e.g., the skin temperature. Figure 11(*a*) presents the design of the hand splint, which follows the 3D scan of the hand. As the liner is often made of soft materials and put in-between the splint and the skin, we took the shape of the hand and the forearm as the design space of the receiver coil. A flat table was taken as the design space of the transmitter coil and the relative position between two design spaces was set to be that the arm was put on the table with the palm facing upwards. With these two design spaces and by setting 0.1 W as the desired power to be transferred, the receiver coil was generated using the proposed method as shown in Fig. 11(*b*). Using LSCM, we mapped the 3D design to 2D and printed the coil on soft thermoplastic polyurethane (TPU) film using a Voltera electronics printer. The coil trace was printed by Voltera FLEX 2 ink using a 225-μm nozzle. The dispense height was set as 0.16 mm for the flexible TPU film. And the feed rate of the nozzle was set as 500 mm/min. After printing, the substrate with the printed trace was cured at 60 °C for 20 min. Figure 11(*c*) shows the printing process and in Fig. 11(*d*), the printed receiver coil is presented. In Fig. 11(*e*), the printed liner (with the receiver coil) was put in the hand splint. As this form, the self-inductance of the coil was measured as 1.01×10^{-6} H, which was 6.93% smaller than the calculation result (1.08×10^{-6} H). In Fig. 11(*f*), we demonstrated the effectiveness of the printed receiver coil by powering an LED. In this experiment, the error between the calculation and the measurement results was much smaller, mainly due to that the coil was digitally fabricated by the electronics printer.

5 Conclusion

In this paper, we presented a computational design approach for designing 3D coils for IPT. Compared to the traditional design method, the coils are designed and optimized in 3D directly with the consideration of the electromagnetic constraints. Simulation and experiment results show that the proposed approach can be a useful method in minimizing the size as well as reducing the use of materials, both contribute to a more efficient design.

Current research is focused towards two directions of printing the designed coils for different applications. In the first direction, we are working on multi-layer conformal printing using thermoforming [49] to increase the power that can be transferred. At the second direction, we are exploring the possibilities of directly printing the 3D coils using 3D printed electronics.

Acknowledgment

The presented research was partially funded by the European Institute of Technology (EIT) AddMANU project and Dutch NWO Next UPPS—Integrated Design Methodology for Ultra Personalised Products and Services project. The work of Mr. Jun Xu was supported by the China Scholarship Council (CSC, No. 201806890022). The author would also like to express their appreciation to Mr. Rick van Veen, Mr. Martin Verwaal, Mr. Adrie Kooijman, Mr. Joris van Dam, and Ms. Tessa Essers for the fruitful discussions and kind assistance during the experiment.

References

[1] Lakhal, H., Dhieb, M., Ghariani, H., and Lahiani, M., 2013, "Wireless Power Transmission Technologies and Applications," 14th International Conference on Sciences and Techniques of Automatic Control & Computer Engineering—STA'2013, Sousse, Tunisia, pp. 168–173.

[2] "History of the QI Specification," 2021, Wireless Power Consortium [Online], https://www.wirelesspowerconsortium.com/knowledge-base/specifications/history-of-the-qi-specification.html

[3] Hou, T., Song, Y., Elkhuizen, W. S., Jiang, J., and Geraedts, J. M. P., 2018, "3D Wireless Power Transfer Based on 3D Printed Electronics," 2018 IEEE 14th International Conference on Automation Science and Engineering (CASE), Munich, Germany, Aug., pp. 499–505.

[4] Huang, Y., Wu, H., Xiao, L., Duan, Y., Zhu, H., Bian, J., Ye, D., and Yin, Z., 2019, "Assembly and Applications of 3D Conformal Electronics on Curvilinear Surfaces," Mater. Horiz., **6**(4), pp. 642–683.

[5] Kim, Y., Kweon, O. Y., Won, Y., and Oh, J. H., 2019, "Deformable and Stretchable Electrodes for Soft Electronic Devices," Macromol. Res., **27**(7), pp. 625–639.

[6] Dagdeviren, C., Su, Y., Joe, P., Yona, R., Liu, Y., Kim, Y. S., Huang, Y., et al., 2014, "Conformable Amplified Lead Zirconate Titanate Sensors With Enhanced Piezoelectric Response for Cutaneous Pressure Monitoring," Nat. Commun., **5**(1), pp. 1–10.

[7] Jeong, J. W., Kim, M. K., Cheng, H., Yeo, W. H., Huang, X., Liu, Y., Zhang, Y., Huang, Y., and Rogers, J. A., 2014, "Capacitive Epidermal Electronics for Electrically Safe, Long-Term Electrophysiological Measurements," Adv. Healthcare Mater., **3**(5), pp. 642–648.

[8] Pang, C., Koo, J. H., Nguyen, A., Caves, J. M., Kim, M. G., Chortos, A., Kim, K., Wang, P. J., Tok, J. B. H., and Bao, Z., 2015, "Highly Skin-Conformal Microhairy Sensor for Pulse Signal Amplification," Adv. Mater., **27**(4), pp. 634–640.

[9] Rendon-Nava, A. E., Díaz-Méndez, J. A., Nino-De-Rivera, L., Calleja-Arriaga, W., Gil-Carrasco, F., and Díaz-Alonso, D., 2014, "Study of the Effect of Distance and Misalignment Between Magnetically Coupled Coils for Wireless Power Transfer in Intraocular Pressure Measurement," Sci. World J., **2014**, pp. 1–11.

[10] Lai, Y. C., Deng, J., Liu, R., Hsiao, Y. C., Zhang, S. L., Peng, W., Wu, H. M., Wang, X., and Wang, Z. L., 2018, "Actively Perceiving and Responsive Soft Robots Enabled by Self-Powered, Highly Extensible, and Highly Sensitive Triboelectric Proximity- and Pressure-Sensing Skins," Adv. Mater., **30**(28), p. 1801114.

[11] Lei, Z., Wang, Q., and Wu, P., 2017, "A Multifunctional Skin-Like Sensor Based on a 3D Printed Thermo-Responsive Hydrogel," Mater. Horiz., **4**(4), pp. 694–700.

[12] Muth, J. T., Vogt, D. M., Truby, R. L., Mengüç, Y., Kolesky, D. B., Wood, R. J., and Lewis, J. A., 2014, "Embedded 3D Printing of Strain Sensors Within Highly Stretchable Elastomers," Adv. Mater., **26**(36), pp. 6307–6312.

[13] Song, Y., Boekraad, R. A., Roussos, L., Adrie, K., Wang, C. C. L., and Geraedts, J. M. P., 2017, "3D Printed Electronics: Opportunities and Challenges for Industrial Designers," 37th Computers and Information in Engineering Conference, Cleveland, OH, pp. 1–11.

[14] Khan, S., Lorenzelli, L., and Dahiya, R. S., 2015, "Technologies for Printing Sensors and Electronics Over Large Flexible Substrates: A Review," IEEE Sens. J., **15**(6), pp. 3164–3185.

[15] Zhang, W., Zhang, L., Liao, Y., and Cheng, H., 2021, "Conformal Manufacturing of Soft Deformable Sensors on the Curved Surface," Int. J. Extrem Manuf., **3**(4), p. 042001.

[16] Jeong, S., Kim, D.-H., Song, J., Kim, H., Lee, S., Song, C., Lee, J., Song, J., and Kim, J., 2019, "Smartwatch Strap Wireless Power Transfer System With Flexible PCB Coil and Shielding Material," IEEE Trans. Ind. Electron., **66**(5), pp. 4054–4064.

[17] Yang, C., Wu, S. Y., Glick, C., Choi, Y. S., Hsu, W., and Lin, L., 2015, "3D Printed RF Passive Components by Liquid Metal Filling," 2015 28th IEEE International Conference on Micro Electro Mechanical Systems (MEMS), Estoril, Portugal, Feb., pp. 261–264.

[18] Iyer, V., Chan, J., and Gollakota, S., 2017, "3D Printing Wireless Connected Objects," ACM Trans. Graph., **36**(6), pp. 1–13.

[19] Ota, H., Emaminejad, S., Gao, Y., Zhao, A., Wu, E., Challa, S., Chen, K., et al., 2016, "Application of 3D Printing for Smart Objects With Embedded Electronic Sensors and Systems," Adv. Mater. Technol., **1**(1), p. 1600013.

[20] Xu, J., Doubrovski, E. Z. L., Geraedts, J. M. P., and Song, Y. W., 2021, "Design 3D Printed Coils for WPT," ASME 2021 International Design Engineering Technical Conferences and Computers and Information in Engineering Conference, Virtual Online, Vol. 85376, p. V002T02A043

[21] Covic, G. A., and Boys, J. T., 2013, "Inductive Power Transfer," Proc. IEEE, **101**(6), pp. 1276–1289.

[22] Rakhymbay, A., Khamitov, A., Bagheri, M., Alimkhanuly, B., Lu, M., and Phung, T., 2018, "Precise Analysis on Mutual Inductance Variation in Dynamic Wireless Charging of Electric Vehicle," Energies, **11**(3), p. 624.

[23] Chen, C., Hu, W., Luo, J., Lei, Y., Tong, Q., Zhang, X., Sang, H., and Xie, C., 2015, "Planar Micro-Nano-Coils for Electrically Driving Liquid Crystal Microlenses Based on Wireless Power Transmission," MIPPR 2015: Multispectral Image Acquisition, Processing, and Analysis, Enshi, China, Vol. 9811, May, p. 981105.

[24] Lemdiasov, R., and Venkatasubramanian, A., 2017, "Transmit Coil Design for Wireless Power Transfer for Medical Implants," 2017 39th Annual International Conference of the IEEE Engineering in Medicine and Biology Society (EMBC), Jeju, South Korea, pp. 2158–2161.

[25] Ha-Van, N., and Seo, C., 2018, "Analytical and Experimental Investigations of Omnidirectional Wireless Power Transfer Using a Cubic Transmitter," IEEE Trans. Ind. Electron., **65**(2), pp. 1358–1366.

[26] Zargham, M., and Gulak, P. G., 2012, "Maximum Achievable Efficiency in Near-Field Coupled Power-Transfer Systems," IEEE Trans. Biomed. Circuits Syst., **6**(3), pp. 228–245.

[27] Eteng, A. A., Rahim, S. K. A., Leow, C. Y., Chew, B. W., and Vandenbosch, G. A. E., 2016, "Two-Stage Design Method for Enhanced Inductive Energy Transmission With Q-Constrained Planar Square Loops," PLoS One, **11**(2), pp. 1–13.

[28] Van Wageningen, D., and Staring, T., 2010, "The Qi Wireless Power Standard," Proceedings of 14th International Power Electronics and Motion Control Conference EPE-PEMC 2010, Ohrid, Macedonia, September, IEEE, pp. 25–32.
[29] Kamyshny, A., and Magdassi, S., 2014, "Conductive Nanomaterials for Printed Electronics," Small, **10**(17), pp. 3515–3535.
[30] Wu, H., Tian, Y., Luo, H., Zhu, H., Duan, Y., and Huang, Y. A., 2020, "Fabrication Techniques for Curved Electronics on Arbitrary Surfaces," Adv. Mater. Technol., **5**(8), pp. 1–29.
[31] Harnois, M., Himdi, M., Yong, W. Y., Rahim, S. K. A., Tekkouk, K., and Cheval, N., 2020, "An Improved Fabrication Technique for the 3-D Frequency Selective Surface Based on Water Transfer Printing Technology," Sci. Rep., **10**(1), pp. 1–8.
[32] Devaraj, H., and Malhotra, R., 2019, "Scalable Forming and Flash Light Sintering of Polymer-Supported Interconnects for Surface-Conformal Electronics," ASME J. Manuf. Sci. Eng., **141**(4), p, 041014.
[33] Yang, Y., Vervust, T., Dunphy, S., Van Put, S., Vandecasteele, B., Dhaenens, K., Degrendele, L., et al., 2018, "3D Multifunctional Composites Based on Large-Area Stretchable Circuit With Thermoforming Technology," Adv. Electron. Mater., **4**(8), p. 1800071.
[34] Lee, S. Y., Jang, S. H., Lee, H. K., Kim, J. S., Lee, S., Song, H. J., Jung, J. W., Yoo, E. S., and Choi, J., 2020, "The Development and Investigation of Highly Stretchable Conductive Inks for 3-Dimensional Printed In-Mold Electronics," Org. Electron., **85**, p. 105881.
[35] Zhou, N., Liu, C., Lewis, J. A., and Ham, D., 2017, "Gigahertz Electromagnetic Structures Via Direct Ink Writing for Radio-Frequency Oscillator and Transmitter Applications," Adv. Mater., **29**(15), p. 1605198.
[36] Boekraad, R., 2017, "3D-Printed Electronics: A Case Study Concerning Wireless Power Transfer," Master thesis, Delft University of Technology, Delft.
[37] Zhu, Z., Guo, S.-Z., Hirdler, T., Eide, C., Fan, X., Tolar, J., and McAlpine, M. C., 2018, "3D Printed Functional and Biological Materials on Moving Freeform Surfaces," Adv. Mater., **30**(23), p. 1707495.
[38] Hou, T., Xu, J., Elkhuizen, W. S., Wang, C. C. L., Jiang, J., Geraedts, J. M. P., and Song, Y., 2019, "Design of 3D Wireless Power Transfer System Based on 3D Printed Electronics," IEEE Access, **7**, pp. 94793–94805.
[39] Tan, W. S., Juhari, M. A. B., Shi, Q., Chen, S., Campolo, D., and Song, J., 2020, "Development of a New Additive Manufacturing Platform for Direct Freeform 3D Printing of Intrinsically Curved Flexible Membranes," Addit. Manuf., **36**, p. 101563.
[40] Sethian, J. A., 1996, "A Fast Marching Level Set Method for Monotonically Advancing Fronts," Proc. Natl. Acad. Sci. USA, **93**(4), pp. 1591–1595.
[41] Crane, K., Weischedel, C., and Wardetzky, M., 2013, "Geodesics in Heat," ACM Trans. Graph., **32**(5), pp. 1–11.
[42] Chen, L., Zhang, R., Tang, K., Hu, P., Zhao, P., Li, Z., and Han, Z., 2020, "A Spiral-Based Inspection Path Generation Algorithm for Efficient Five-Axis Sweep Scanning of Freeform Surfaces," Comput. Aided Des., **124**, p. 102838.
[43] Nehari, Z., 1952, *Conformal Mapping*, McGraw-Hill, New York.
[44] Wang, S., Wang, Y., Jin, M., Gu, D., and Samaras, D., 2007, "Conformal Geometry and Its Applications on 3D Shape Matching, Recognition, and Stitching," IEEE Trans. Pattern Anal. Mach. Intell., **29**(7), pp. 3653–3667.
[45] Li, W., Yin, Z., Huang, Y., Wu, T., and Xiong, Y., 2011, "Tool Path Generation for Triangular Meshes Using Least-Squares Conformal Map," Int. J. Prod. Res., **49**(12), pp. 3653–3667.
[46] Pomplun, M., Ritter, H., and Velichkovsky, B., 1996, "Disambiguating Complex Visual Information: Towards Communication of Personal Views of a Scene," Perception, **25**(8), pp. 931–948.
[47] Masoudi, N., Fadel, G. M., and Wiecek, M. M., 2020, "Planning the Shortest Path in Cluttered Environments: A Review and a Planar Convex Hull-Based Approach," ASME J. Comput. Inf. Sci. Eng., **19**(4), p. 041011.
[48] Budnik, K., and Machczyński, W., 2012, "Inductances of Coaxial Helical Conductors," Comput. Appl. Electr. Eng., **10**, pp. 358–371.
[49] Chen, S. C., Huang, S. T., Lin, M. C., and Chien, R. D., 2008, "Study on the Thermoforming of PC Films Used for In-Mold Decoration," Int. Commun. Heat Mass Transfer, **35**(8), pp. 967–973.